Asian Journal of Chemistry; Vol. 34, No. 11 (2022), 2806-2812

ASIAN JOURNAL OF CHEMISTRY

https://doi.org/10.14233/ajchem.2022.23764

Excellent Red Phosphors of Eu^{3+} Activated Double Perovskite Structured Series $NaSrBi_{1-x}Eu_xMoO_6$ (x = 0.0-0.24) Prepared by Citrate-Gel Method

K. Koteswara Rao and B. Nagamani Naidu*

Department of Basic Science & Humanities, GMR Institute of Technology (Affiliated to Jawaharlal Nehru Technological University Kakinada), Rajam-532127, India

*Corresponding author: E-mail: nagamaninaidu.b@gmrit.edu.in

Received: 4 February 2022; *Accepted*: 14 May 2022; *Published online*: 19 October 2022; AJC-20989

In this work, a double perovskite structured series was prepared by using simple citrate sol-gel method at 700 ºC for 5 h of sintering. The concentrated sample of x = 0.12 exhibits more intensity than all other concentration in their emission spectra for every series. Particle size, thickness of the particle, distance between particles and its surface morphology were identified by scanning electron microscopy. The size and distance between particles in each series lies in between the range of 1 µm-50 nm and 20-50 nm, respectively. Many voids with strong agglomerations were also observed. In addition, the absorption of light capacity for each series investigated through diffuse reflectance spectra method. All the samples of double perovskite structures exhibit a sharp cut-off of absorption light in the UV-visible regions of diffuse reflectance spectra. Predominantly, all the samples shows a very good charge transfer band in their excitation spectra that leads to more absorption of light correspondingly emits high intensity in emission spectra at 395, 464 and 545 nm. All the samples of every series emit main peaks in the range of 550-700 nm in their emission spectra. Out of all four main peaks, 614 nm peak represents the red phosphor with $^5D_0$-$^7F_2$ transition in the emission spectra. The prepared double perovskite structure compound CRI coordinates were almost close to commercially available red phosphor *i.e.* Y_2O_2S(0.67,0.33) as per NTSC. Hence, the prepared red phosphors can be used in order to display devices, luminescent materials and WLEDs.

Keywords: Sol-gel method, Luminescence, Bismuth molybdate, Energy transfer, Red phosphor.

INTRODUCTION

Several scientists are working constantly on the phosphors, since they mostly used in all areas but mainly are used in manufacture of white light emitting diodes (WLEDs). These WLEDs are very important commercial materials due to their special characteristics like long life time, economically low-cost, high efficacy and little amount of toxic nature [1,2]. In order to produce white light generation three methods are followed [3,4]. They are (i) mixing of three monochromatic light sources red, green and blue; (ii) excitation of blue, red and green phosphors coated on an epoxy with blue UV LED; and (iii) combination of blue LED chip with yellow phosphor. Since, the efficiency of red light is eight times less than the green and blue light [5]. So, the researchers are focused to improve the efficiency of red light. There are many other red phosphor materials, which are available in the market mainly oxides, sulphides, *etc*. form, even though red phosphor material containing sulphide has high efficient, but it has less life time and highly toxic in nature [6,7]. However, double perovskite structured materials are mainly substitued in the preparation of WLEDs. Researchers continually trying to improve the efficiency of red component by using double perovskite structured materials which are majorly used in the electronic, ferrites, photonics [8-11], photocatalysts [12-20], *etc*. Similarly, molybdate and tungstate are also tried in these double perovskite structures as main elements to improve the red light efficacy due to their high thermal and chemical stability [21].

Similarly, due to their specific characterstics like a good lumin equivalent, quantum efficiency, photostability and well defined transitions, the rare earth element ions are also used in WLEDs [22]. Generally, Eu^{3+} ions exhibit $^5D_0$-^7E_J transitions, where $^5D_0$-$^7F^1$ (595 nm) and $^5D_0$-$^7F_2$ (614 nm) are the strong transitions, which comes under the red region [22]. Moreover, Eu^{3+} ions have good absorption capacity, high colour purity and also exhibit stable chemical and physical properties [23,24].

In this work, a double perovskite with bismuth as one of the host elements is well known energy transfer centre and environmentally safe element [25], apart from its low price and large availability in nature is reported. By substituting bismuth ions in place of gadolinium, for the double perovskite composition [26], a similar change is expected insite symmetry and in view of its inherent energy transfer behaviour could additionally help in obtaing higher emission efficiency. Earlier, we have prepared Eu^{3+} doped Bi_2MoO_6 by a semi sol-gel method and found good red luminescence intensity [27]. Encouraged by these results, a new bimuth containing double perovskite of composition $NaSrBi_{1-x}Eu_xMoO_6:Eu^{3+}$ is prepared by a sol-gel method and characterized its crystal structure and luminescence properties as a function of dopant concentration.

EXPERIMENTAL

Synthesis: A series of $NaSrBi_{1-x}Eu_xMoO_6:Eu^{3+}$ ($x = 0.0$-0.24) phosphors was prepared by following a sol-gel method using AR grade starting materials $NaNO_3$, $Sr(NO_3)_2$, Bi_2O_3, Eu_2O_3, $(NH_4)_6Mo_7O_{24}{\cdot}4H_2O$, HNO_3 and citric acid procured from the reliable commercial sources.

The preparation of $NaSrBi_{0.88}Eu_{0.12}MoO_6:0.12Eu^{3+}$, the usual procedure for the sample preparation is illustrated as follows: Weighed the required amount of starting materials *i.e.* 0.8696 g of $NaNO_3$, 2.1842 g of $Sr(NO_3)$, 2.1136 g of Bi_2O_3, 0.2179 g Eu_2O_3, as per stoichiometry and transferred to 500 mL glass beaker. Added distilled water slowly to all the starting materials to get a clear solution. If any sample is not dissolved in distilled water, added either nitric acid or liquefied ammonia in a minimum quantity. After that, the solution should maintain its pH at around 6-7 by adding required amount of either acid or base to the solution. The total quantity of the solution should not exceed 300 mL and then place on the magnetic stirrer, which contains two nobs for simultaneous heating as well as stirring. This solution is subjected to the magnetic stirrer for 6-8 h at 100 ºC. Then, before formation of a grey gel liquid, added ethylene glycol (1.5 mL) dropwise to the solution mixture. After 8 h of simultaneous heating and stirring, a grey gel was formed. The gel was burned in an electric burner for 15-20 min. The grey powder form was grinded in mortar pestle to get the fine powder, then annealed at various temperatures *viz*. 500 ºC, 600 ºC and 700 ºC for 5 h in a muffle furnace to obtain a red light emitting phosphor.

Characterization: The XRD patterns were recorded by using X-ray Diffractrometer (Phillips PW 1830) with Cu$K\alpha$ radiation (K = 0.15406 Å) at 36 kV tube voltage and 20 mA tube current. On the other hand, the angles (2θ) values were recorded for every structure in between 100-900 with 0.02 scanning speed and 40/min scanning rate, respectively. The light absorbance capacity was measured with diffuse reflectance spectra (Perkin-Elmer UV Win lab 6.2). The surface morphology, size and distance between particles were measured with FESEM (Oxford instruments). The excitation and emission spectra were recorded by using PL data (FP8300,Serial number D046261450). The CRI co-ordinates were measured by using Osram Sylvania color calculator.

RESULTS AND DISCUSSION

X-ray diffraction (XRD) studies: The double perovskite samples have been synthesized by sol-gel method, at various temperatures *i.e.* 500, 600 and 700 ºC for 5 h of each series. The XRD patterns exhibit impurities as well as double perovskite phases. However, the sample annealed at 700 ºC for 5 h exhibits purified, perfect, well-matched crystal structure. Annealing beyond 700 ºC for 5 h, the partial melting of the samples was observed.Thus, the optimum temperature for the preparation of red phosphor compounds is at 700 ºC for 5 h.

The powder-XRD patterns of all the samples in the series $NaSrBi_{1-x}Eu_xMoO_6$ ($x = 0.0$-0.24) are shown in Fig. 1. For the concentration of Eu^{3+} ranging from 0.0 to 0.03, the XRD data of double perovskite samples, fits well with orthorohmbic phase having space group: *Pban*. These compounds have well matched peak patterns with earlier reported (JCPDS No. 24-0423) [28]. The lattice parameters of a representative orthorohmbic sample ($x = 0.0$-0.03) were $a = 10.8107$ Å, $b = 11.9599$, $c = 8.9062$, V = 1151.53 Å^3. For Eu^{3+} concentration ranging between 0.12 to 0.18, the powder patterns showed monoclinic phases with space group $P2/m$ and the lattice parameters were $a = 10.5106$ Å, $b = 4.9922$ Å, $c = 8.1849$ Å, V = 402.54 Å^3. The XRD patterns of $NaSrBi_{1-x}Eu_xMoO_6$ ($x = 0.21$-0.24) showed the triclinic crystal structure with space group of $P\bar{1}$.

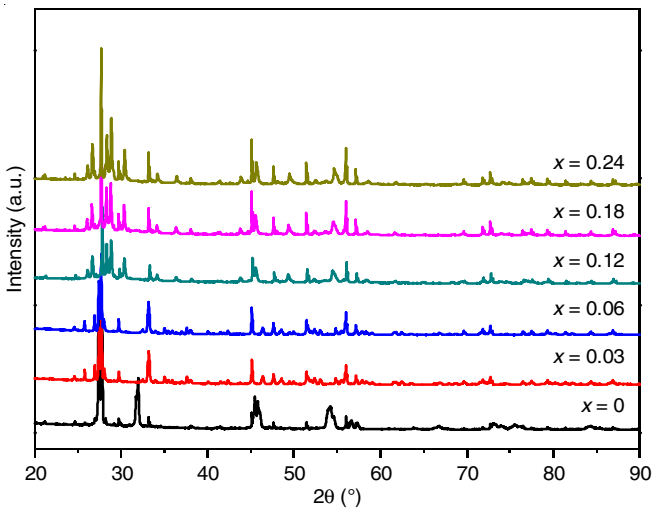

Fig. 1. Powder XRD patterns of samples $NaSrBi_{1-x}Eu_xMoO_6$ for $x = 0.03$-0.24

Diffuse reflectance spectra (DRS): The efficiency of any phosphor depends on the nature of host crystal lattice and doped rare earth ion activator. Host lattice absorbs the light and transfers to doped rare earth ion activator. Either host crystal lattice or doped rare earth ion activator absorbs light radiation alone, if so a lead to very low emission intensity is observed in the phosphors material [29,30]. Additionally, diffuse reflectance spectra explains the band gap of host crystal lattice, which is also one of the factors to influence the absorbance capacity of material [31,32].

From DRS spectra (Fig. 2), a good absorption intensity at the lower wavelengths and the absorption intensity decreases as moved to longer wavelengths is observed. The absorbance

capacity of phosphor appear in two regions. The first region of absorbance band ranging from 200-380 nm due to the oxygen-Mo charge transfer transition [33], while the second region ranged from 400-480 nm is due to *f-f* transition of Eu^{3+}, which is a weak absorption band. The prepared sample exhibited strong absorption in UV region as well as very weak absorption in near UV region. Moreover, a steep fall of absorbance spectra occured around 400-450 nm is due to the band gap transition, but not due to the crystal defects in host lattice structure [34].

FE-SEM studies: For sample of $x = 0.12$, the prepared sample exhibits the sharp flake like structures with strong agglomerations and the particle size ranging on average from 20-30 nm and the distance between particle lies in between 100-200 nm. Fig. 3 shows the EDAX profile of $NaSrBi_{1-x}Eu_xMoO_6$ ($x = 0.12$). The presence of all elements as per the sample composition is quite visible from the spectra and the stoichiometric ratio of elements were found to be close to the intended stoichiometry of the prepared sample ($x = 0.12$). The commer-

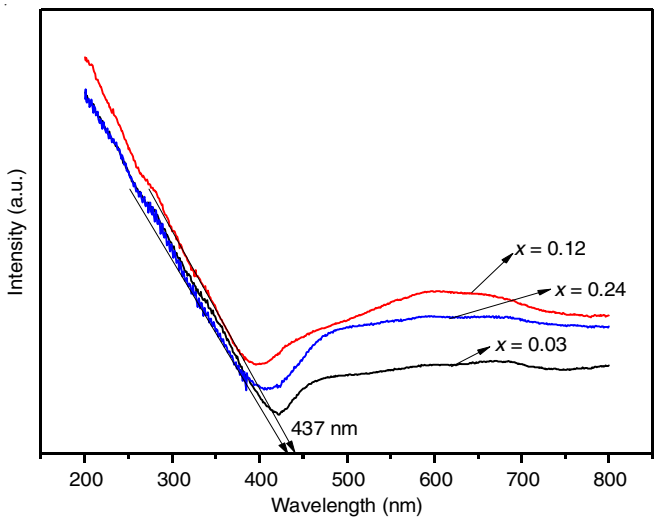

Fig. 2. UV-Vis reflectance spectra for $NaSrBi_{1-x}Eu_xMoO_6$ for $x = 0.03$-0.24 with different Eu^{3+}concentrations

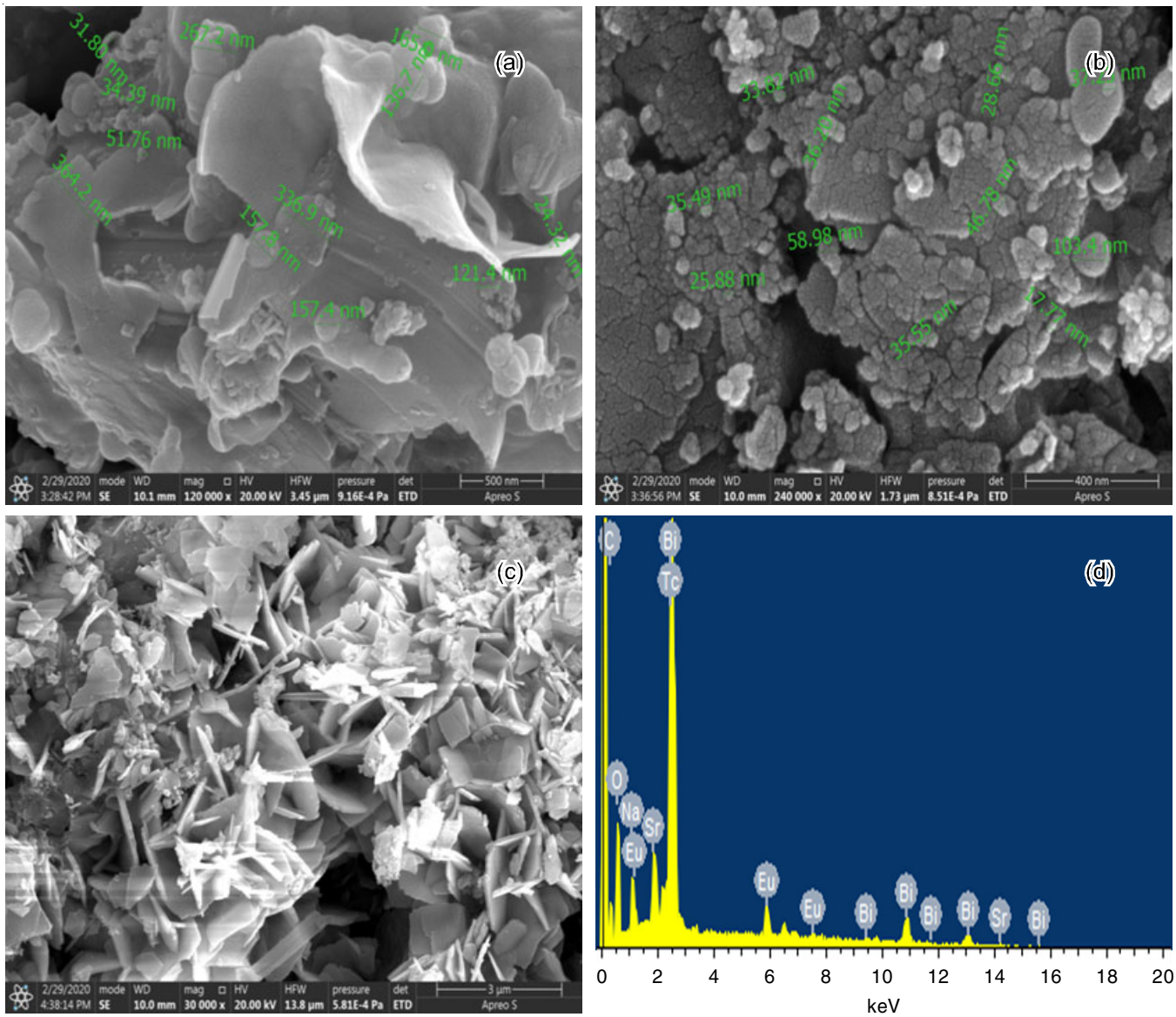

Fig. 3. SEM images of $NaSrBi_{1-x}Eu_xMoO_6$:Eu^{3+} at (a) 1 µm, (b) 400 nm, (c) 100 nm, (d) EDAX pattern for $NaMgBi_{1-x}Eu_xMoO_6$:Eu^{3+}

cial phosphor samples usually possesses particles sizes in the range 2-10 μm [35]. The prepared phosphor consists both the nano and micron sizes, and hence the emission intensities would be comparable to the commercial red phosphors.

The as-prepared particles were dispersed into deionized water and particle size was measured by particle size analyzer (PSA) using Fraunhofer method. The morphologies of the double-perovskite did not vary with different doping concentration. Several voids were observed in the morphologies, which might be due to the inadequate sintering temperature profile. Since the optimum condition for synthesis this phosphor has not been known yet and the particle size, morphology and voids affect the luminescence properties, it is expected that the photoluminescence properties will be improved by the appropriate sintering temperature profile.

CIE coordinates of the phosphors: The color purity and the chromoticity co-ordinators (*x*,*y*) of any phosphor material are measured with CIE (Commission International D'E Clairage) software (CIE 1931 XY.V.1.6.0.2) by using photoluminescence data of the prepared phosphor materials. The CIE mode is connected to software link, where the photoluminescence data *i.e*. wavelength and colour observed were incorporated, in order to find out the colour the purity and the chromaticity co-ordinators (*x*,*y*). However, the prepared red phosphor chromaticity co-ordinators (*x*,*y*) have been measured using the above said software and the data is given in Table-1.

For sample $NaSrBi_{1-x}Eu_xMoO_6:Eu^{3+}$ ($x = 0.12$), the (*x*,*y*) is (0.6298,0.3702), (X_d,Y_d) is (0.66,0.32) and (X_i,Y_i) is (0.31,0.32). Thus, the colour purity for the prepared sample is 91.4%, which shows the sample falls in the red region and also the CCT values are also lies around 1200-1500K, for all the different concentrations of the $NaSrBi_{1-x}Eu_xMoO_6$ for $x = 0.03$-0.24.

The obtained results of chromaticity co-ordinators (*x*,*y*) are closed to the standard red phosphor, *i.e*. (0.67,0.33). On the other hand, the sample with $x = 0.12$ shows very close to the chromaticity co-ordinators of the commercial standard red phosphor for every series. Moreover, the obtained co-ordinators

TABLE-1
CIE CO-ORDINATES OF $NaSrBi_{1-x}Eu_xMoO_6$ FOR ($x = 0.03$-0.24) FROM EMISSION SPECTRA EXCITED AT 465 nm

Sample	CIEx (465 nm)	CIEy (465 nm)	CCT (K)
$NaSrBi_{0.97}Eu_{0.03}MoO_6:Eu^{3+}$	0.6191	0.3808	1382
$NaSrBi_{0.91}Eu_{0.09}MoO_6:Eu^{3+}$	0.6214	0.3786	1248
$NaSri_{0.88}Bi_{0.88}Eu_{0.12}MoO_6:Eu^{3+}$	0.6298	0.3702	1195
$NaSrBi_{1.82}Eu_{0.18}MoO_6:Eu^{3+}$	0.6204	0.3796	1276
$NaSrBi_{1.79}Eu_{0.21}MoO_6:Eu^{3+}$	0.6119	0.3881	1387
$NaSrBi_{1.76}Eu_{0.24}MoO_6:Eu^{3+}$	0.6059	0.3941	1498

are very close to the CIE edge in the CIE diagram (Fig. 4), it indicates that the luminescence intensity and colour purity of prepared phosphor can be optimized by increasing the concentration of Eu^{3+} dopant gradually.

By gradual increment of Eu^{3+} dopants into the host crystal lattice, the ratio of R/O increases and leads to terminate the symmetric nature of the prepared red phosphor. Hence, the red colour purity, emission intensity and the availability of different excitation chips can be optimized. Similarly, the colour tone of the prepared red phosphor changes with the increasing of Eu^{3+} ion concentration. It varies from yellowish orange to orange reddish and finally turns to red colour tone. Once the colour tone is optimized, it can't be changed with the gradual increment of Eu^{3+} dopant concentration. The colour purity (CP) of the prepared sample can be measured using below equation [36,37]:

$$CP = \frac{\sqrt{(x - x_i)^2 + (y - y_i)^2}}{\sqrt{(x_d - x_i)^2 + (y_d - y_i)^2}}$$

where (*x*,*y*) are the prepared sample coordinators, (X_d,Y_d) are the dominant wavelength co-ordinators and (X_i,Y_i) are the standard white light coordinators.

Photoluminescence (PL) studies: Fig. 5 shows the excitation spectra for $NaSrBi_{1-x}Eu_xMoO_6:Eu^{3+}$ ($x = 0.0$-0.24) prepared at 700 ºC for 5 h by sol-gel method. The charge transfer

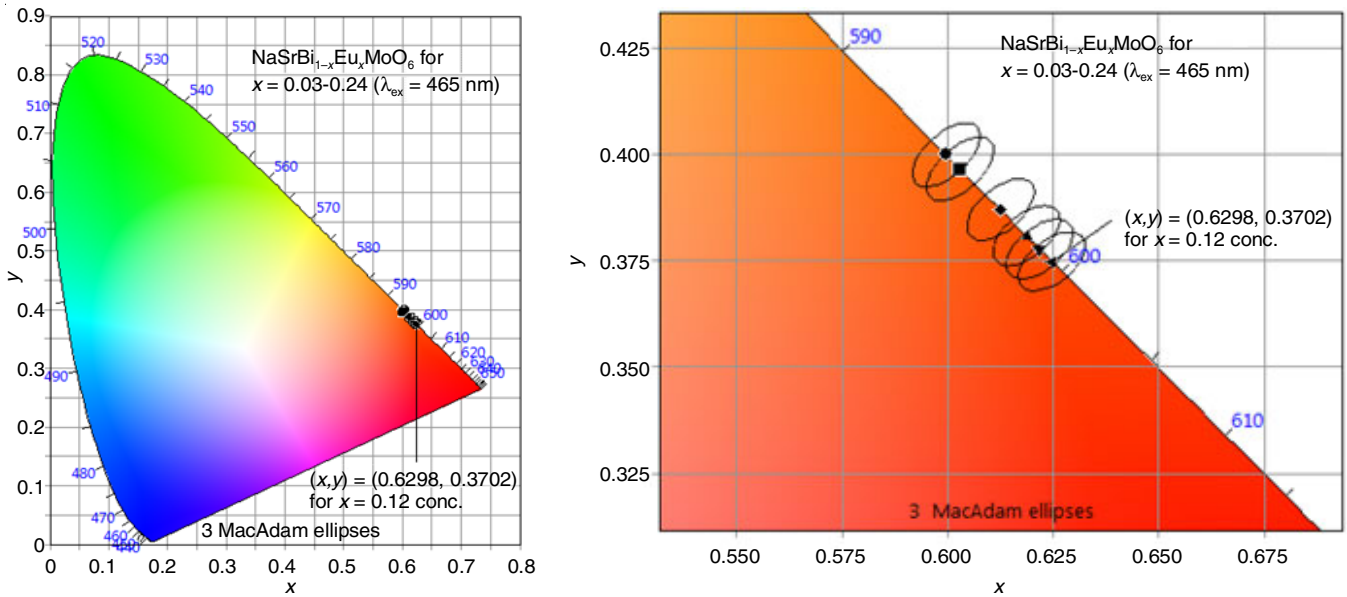

Fig. 4. CIE chromaticity coordinates of $NaSrBi_{1-x}Eu_xMoO_6$ for $x = (0.03$-$0.24)$ ($\lambda_{ex} = 465$ nm)

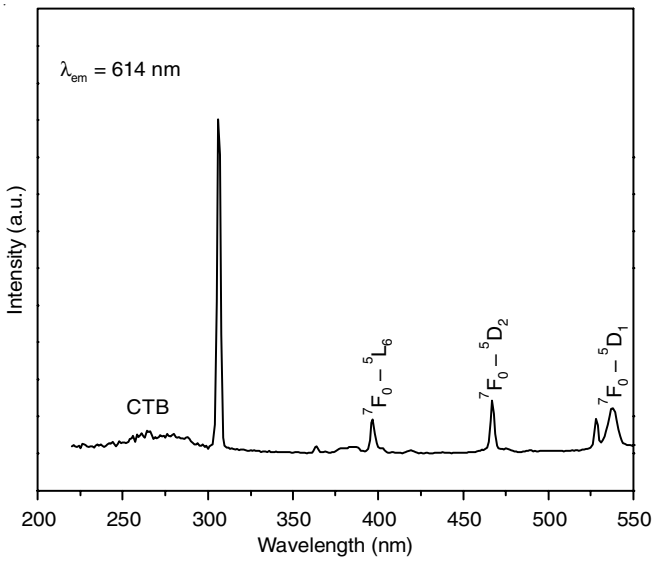

Fig. 5. Excitation spectra of $NaSrBi_{1-x}Eu_xMoO_6$ (x = 0.12) obtained by monitoring 614 nm emission

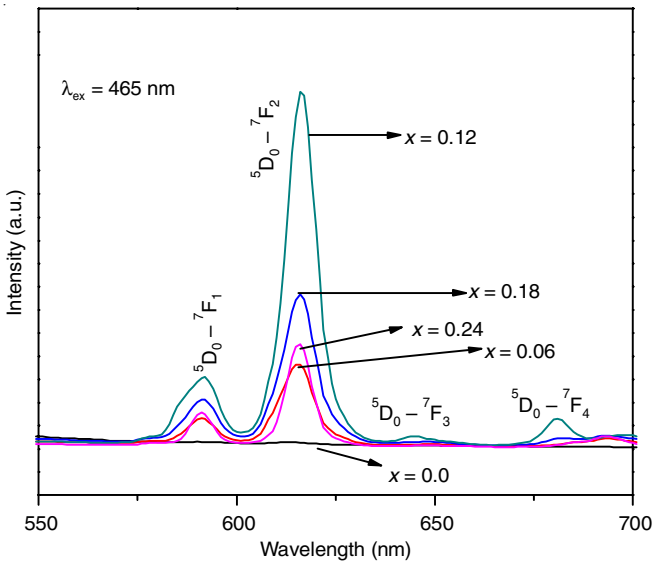

Fig. 6. Emission spectra of $NaSrBi_{1-x}Eu_xMoO_6$ (x = 0.03-0.24) obtained by exciting at 465 nm

band (CTB) lies in the range of 250-350 nm, due to Mo^{6+}–O, Eu^{3+}–O transitions [38]. In general, high intensified CTB transition represents more absorption of light; correspondingly it transfers the light energy to luminescent centre, which leads to emit high emission intensity radiation.

The concentrated sample at x = 0.12 considered as the optimum concentration level for recording excitation as well as emission spectra for the sample $NaSrBi_{1-x}Eu_xMoO_6$:Eu^{3+} at various wavelength. Diffuse reflectance spectra also supports the optimum concentration of x = 0.12, by showing the systematic red shift of absorption edge with increase concentration from x = 0.12-0.12. The sharp peaks were appeared at 395, 467, 540, 595 nm wavelength correspond to $^7F_0$-$^5L_6$, $^7F_0$-$^5D_2$, $^7F_0$-$^5D_1$, $^7F_0$-$^5D_0$ transitions, respectively. Out of these four peaks, relatively a wavelength peak at 467 nm has prominent absorption, which gives high intensity emission at 614 nm.

Emission spectra: Fig. 6 shows the emission spectra for the compound prepared at 700 ºC for 5 h recorded at 395, 467 and 540 nm excited wavelengths. The corresponding emission peaks were assigned as $^5D_0$-^7F_J (J = 0,1,2,3). Out of all four transitions, $^5D_0$-$^7F_2$ transition shows the highest intensity for sample x = 0.12, due to the non-centro symmetric nature of Eu^{3+} in the host crystal lattice [39]. The other transitions, which are formed at 595,650 and 700 nm are to be considered as moderate weak and very weak. Thus, the transition $^5D_0$-$^7F_2$ represents very good red light emission phosphor at 614nm, which is also supported by Li *et al*. [40,41]. Similarly, the XRD pattern also supports the maximum emission intensity for the sample x = 0.12, since, it possess mixed phase structure, which leads to the non-centro symmetric resulting a high emission intensity.

The concentration quenching of the prepared phosphor indicated that as the concentration of Eu^{3+} ions increases, the intensity of $^5D_0$-$^7F_2$ emission transition increases gradually (Fig. 7). Moreover, at x = 0.12 of Eu^{3+} concentration, it attains the maximum intensity. However, beyond x = 0.12 concentration of Eu^{3+}, the intensity of emission transition is declined gradually.

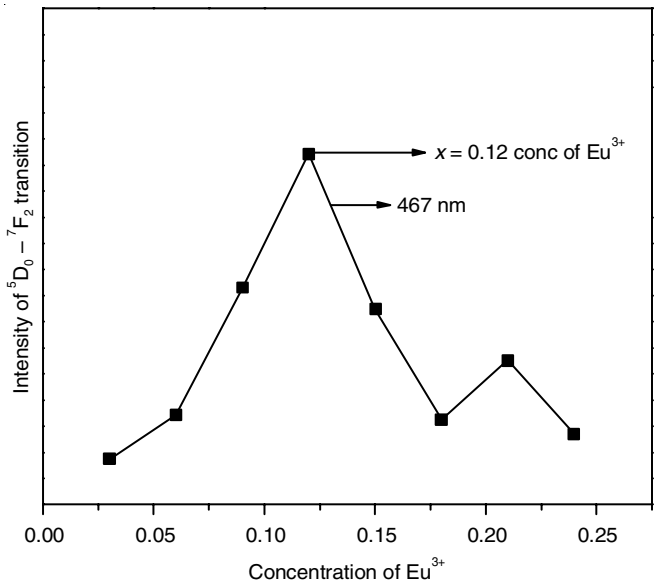

Fig. 7. Comparison of emission intensities (for $^5D_0$–$^7F_2$ transition) as a function of Eu^{3+} conc. for the $NaSrBi_{1-x}Eu_xMoO_6$ (x = 0.03-0.24) excited at 467 nm

The concentration quenching is well explained by Blasse *et al.* [42,43] with critical distance and can be represented as:

$$R_c = 2\left(\frac{3V}{4\pi X_c N}\right)^{1/3}$$

where R_c = critical distance, V = unit cell volume, X_c = critical concentration, N = number of formula units in the unit cell. As V = 947.56 Å^3, X_c = 0.12 and N = 8, the critical distance R_c = 12.35 Å. Since, the critical distance is greater than 5 Å, the non-radiative path way energy transfer is prevalent among the Eu^{3+} ions in the crystal lattice. It also indicates that the multipole-multipole interaction is more dominant and is the major cause of concentration quenching of Eu^{3+} in the phosphors [44].

Moreover, the concentration quenching depends mainly on the energy transfer between the ions in the host crystal lattice, which in turn depends on the distance between the ions in the host crystal lattice. The distance of Eu^{3+}-Eu^{3+} ions varies in different layers of the host material. However, Eu^{3+}-Eu^{3+} ions in the same layer have low range of distance than the ions present in the different layers of the host crystal lattice. Similarly, the distance between Eu^{3+}-Eu^{3+} ions is very low along the *a*-axis, when compared to the *b*- and *c*-axis. Hence, it takes more energy transfer in the same layer along *a*-axis in the host crystal lattice. The reason is well attributed due to the Dexter theory [45], where the concentration quenching causes mainly due to the energy transfer among the ions present in the host crystal lattice and the energy transfer easily takes place between the identical ions, where one of the ions acts like sink due to its existence next to a defect [45].

Conclusion

A series of samples of composition $NaSrBi_{1-x}Eu_xMoO_6$ (x = 0.0-0.24) were prepared by a citrate-gel precursor method. Samples crystallized in orthorhombic, monoclinic and triclinic structures as the concentration of Eu was increased and confirmed by powder XRD. The morphology of samples is flake like structure with particulate inclusions as well having size ranges of few nm to microns, as identified by SEM analysis. The emission spectra recorded by exciting at 467 nm, showed maximum intensity at 614 nm for x = 0.12 in the series of $NaSrBi_{1-x}Eu_xMoO_6$. The color purity and chromaticity co-ordinates are close to standard red light in the CIE diagram, and therefore, useful in WLEDs.

CONFLICT OF INTEREST

The authors declare that there is no conflict of interests regarding the publication of this article.

REFERENCES

1. C. Shivakumara and R. Saraf, *Opt. Mater.*, **42**, 178 (2015); https://doi.org/10.1016/j.optmat.2015.01.006
2. D. Lozano-Mandujano, J. Zárate–Medina, R. Morales-Estrella and J. Muñoz-Saldaña, *Ceram. Int.*, **39**, 3141 (2013); https://doi.org/10.1016/j.ceramint.2012.09.095
3. A.A. Setlur, R.J. Lyons, J.E. Murphy, N.P. Kumar and M.S. Kishore, *ECS J. Solid State Sci. Technol*., **2**, R3059 (2013); https://doi.org/10.1149/2.009302jss
4. J.H. Chen, W.R. Zhao, J.Q. Wang, N.H. Wang, Y.J. Meng, J. He and X. Zhang, *Ceram. Int.*, **41**, 11945 (2015); https://doi.org/10.1016/j.ceramint.2015.06.006
5. D.A. Hakeem, D.H. Kim, S.W. Kim and K. Park, *Dyes Pigments*, **163**, 715 (2019); https://doi.org/10.1016/j.dyepig.2018.12.045
6. Q.T. Zhang, L. Zhang, P.D. Han, Y. Chen, H. Yang and L.X. Wang, *Huaxue Jinzhan*, **23**, 1108 (2011).
7. R. Cao, C. Liao, F. Xiao, G. Zheng, W. Hu, Y. Guo and Y. Ye, *Dyes Pigments*, **149**, 574 (2018); https://doi.org/10.1016/j.dyepig.2017.11.023
8. L. Zhang, Z. Lu, P. Han, L .Wang, Q. Zhang, *J. Mater. Chem. C*, **1**, 54 (2013); https://doi.org/10.1039/C2TC00189F
9. P.F.S. Pereira, A.P. de Moura, I.C. Nogueira, M.V.S. Lima, E. Longo, P.C. de Sousa Filho, O.A. Serra, E.J. Nassar and I.L.V. Rosa, *J. Alloys Compd.*, **526**, 11 (2012); https://doi.org/10.1016/j.jallcom.2012.02.083
10. D.F. Peng, H.Q. Sun, X.S. Wang, J.C. Zhang, M.M. Tang and X. Yao, *J. Alloys Compd.*, **511**, 159 (2012); https://doi.org/10.1016/j.jallcom.2011.09.019
11. M.M. Haque, M.A. Asraf, M.F. Hossen, M.S. Hossan, D.K. Kim and H.I. Lee, *Alloys Comp.*, **539**, 195 (2012); https://doi.org/10.1016/j.jallcom.2012.05.058
12. A. Dias, M.M. Lage, L.A. Khalam, M.T. Sebastian and R.L. Moreira, *Chem. Mater.*, **23**, 14 (2011); https://doi.org/10.1021/cm1027964
13. S.M. Rao, J.K. Srivastava, H.Y. Tang, D.C. Ling, C.C. Chung, J.L. Yang, S.R. Sheen and M.K. Wu, *J. Cryst. Growth*, **235**, 271 (2002); https://doi.org/10.1016/S0022-0248(01)01793-6
14. M. Sadakane, T. Horiuchi, N. Kato, K. Sasaki and W. Ueda, *J. Solid State Chem.*, **183**, 1365 (2010); https://doi.org/10.1016/j.jssc.2010.04.012
15. D. Li, J. Zheng and Z. Zou, *J. Phys. Chem. Solids*, **67**, 801 (2006); https://doi.org/10.1016/j.jpcs.2005.10.182
16. W.H. Eng, P.W. Barnes, B.M. Auer and P.M. Woodward, *J. Solid State Chem.*, **175**, 94 (2003); https://doi.org/10.1016/S0022-4596(03)00289-5
17. Y. Huang and H.J. Seo, *J. Electrochem. Soc.*, **158**, J215 (2011); https://doi.org/10.1149/1.3585838
18. X. Zhang, Z. Li, H. Zhang, S. Ouyang and Z. Zou, *J. Alloys Compd.*, **469**, L6 (2009); https://doi.org/10.1016/j.jallcom.2008.01.117
19. Z. Xia, J. Sun, H. Du, D. Chen and J. Sun, *J. Mater. Sci.*, **45**, 1553 (2010); https://doi.org/10.1007/s10853-009-4123-2
20. M. Irshad, Q.T. Ain, M. Zaman, M.Z. Aslam, N. Kousar, M. Asim, M. Rafique, K. Siraj, A.N. Tabish, M. Usmand, M.H. Farooq, M.A. Assiri and M. Imran, *RSC Adv*., **12**, 7009 (2022); https://doi.org/10.1039/D1RA08185C
21. Z.X. Chen, Y. Chen and Y.S. Jiang, *J. Phys. Chem. B*, **106**, 9986 (2002); https://doi.org/10.1021/jp013301j
22. V. Sivakumar and U.V. Varadaraju, *J. Electrochem. Soc.*, **154**, J28 (2007); https://doi.org/10.1149/1.2382266
23. V.B. Pawade, N.S. Dhoble and S.J. Dhoble, *Mater. Res. Express*, **2**, 095501 (2015); https://doi.org/10.1088/2053-1591/2/9/095501
24. Q. Wan, P.Y. He, N. Dai and B.S. Zou, *Sci. China B Chem.*, **52**, 1104 (2009); https://doi.org/10.1007/s11426-009-0171-3
25. Y. Liang, H.M. Noh, W. Ran, S.H. Park, B.C. Choi, H. Jeong and K.H. Kim, *J. Alloys Compd.*, **716**, 56 (2017); https://doi.org/10.1016/j.jallcom.2017.05.027
26. G. Bühler and C. Feldmann, *Angew. Chem. Int. Ed. Engl.*, **45**, 4864 (2006); https://doi.org/10.1002/anie.200600244
27. B.N. Naidu, K.K. Rao and M.P.S. Murali Kris, *Optik*, **182**, 565 (2019); https://doi.org/10.1016/j.ijleo.2019.01.086
28. H.-D. Nguyen, S.-J. Kim, I.-H. Yeo and S. Mho, *J. Electrochem. Soc.*, **159**, J54 (2012); https://doi.org/10.1149/2.046203jes
29. G. Wenfeng, H. Li, H. Ma and W. Teng, *J. Chem.*, **2014**, 436485 (2014); https://doi.org/10.1155/2014/436485
30. Y. Liu, W. Luo, R. Li, G. Liu, M.R. Antonio and X. Chen, *J. Phys. Chem. C*, **112**, 686 (2008); https://doi.org/10.1021/jp077001z
31. A.K. Parchur and R.S. Ningthoujam, *RSC Adv.*, **2**, 10859 (2012); https://doi.org/10.1039/c2ra22144f
32. J. Zhang, Y. Liu, L. Li, N. Zhang, L. Zou and S. Gan, *RSC Adv.*, **5**, 29346 (2015); https://doi.org/10.1039/C5RA03913D.
33. L. Zhang, T. Xu, X. Zhao and Y. Zhu, *Appl. Catal. B*, **98**, 138 (2010); https://doi.org/10.1016/j.apcatb.2010.05.022
34. J. Zhang, B. Han, P. Li, J. Li and Y. Bian, *Opt. Spectrosc.*, **118**, 735 (2015); https://doi.org/10.1134/S0030400X15050082
35. S. Ye, C.H. Wang, Z.S. Liu, J. Lu and X.P. Jing, *Appl. Phys. B*, **91**, 551 (2008); https://doi.org/10.1007/s00340-008-3028-0

36. F.W. Mo, P.C. Chen, A.X. Guan, X.G. Zhang, C.Y. Xu and L.Y. Zhou, *Ceram. Int.*, **41**, 707 (2015); https://doi.org/10.1016/j.ceramint.2014.08.126
37. G.F. Li, Y.G. Wei, Z.M. Li and G. Xu, *Opt. Mater.*, **66**, 253 (2017); https://doi.org/10.1016/j.optmat.2017.02.018
38. G. Blasse and B.C. Grabmaier, Luminescent Materials, Springer-Verlag: Berlin (1994).
39. C.C. Wu, K.B. Chen, C.S. Lee, T.M. Chen and B.M. Cheng, *Chem. Mater.*, **19**, 3278 (2007); https://doi.org/10.1021/cm061042a
40. Y. Li and X.H. Liu, *Opt. Mater.*, **42**, 303 (2015); https://doi.org/10.1016/j.optmat.2015.01.018
41. J. Hou, X. Yin, Y. Fang, F. Huang and W. Jiang, *Opt. Mater.*, **34**, 1394 (2012); https://doi.org/10.1016/j.optmat.2012.02.031
42. J.Y. Sun, J.H. Zeng, Y.N. Sun, J.C. Zhu and H.Y. Du, *Ceram. Int.*, **39**, 1097 (2013); https://doi.org/10.1016/j.ceramint.2012.07.032
43. G. Blasse, *Phys. Lett. A*, **28**, 444 (1968); https://doi.org/10.1016/0375-9601(68)90486-6
44. Z.H. Wang, Y.H. Hu, S.A. Zhang and J. Lin, *Appl. Phys., A Mater. Sci. Process.*, **122**, 76 (2016); https://doi.org/10.1007/s00339-015-9587-0
45. D.L. Dexter and J.H. Schulman, *J. Chem. Phys.*, **22**, 1063 (1954); https://doi.org/10.1063/1.1740265